European Association for the
Development of Renewable Energies, Environment
and Power Quality (EA4EPQ)

International Conference on Renewable Energies and Power Quality
(ICREPQ'12)
Santiago de Compostela (Spain), 28th to 30th March, 2012

Sizing and Control of the Electric Power Take Off for a Buoy Type Point Absorber Wave Energy Converter

V.C. Tai[1], P.C. See[1], S. Merle[2], and M. Molinas[1]
[1] Department of Electric Power Engineering
Norwegian University of Technology and Science
7941 Trondheim (Norway)
Phone/Fax number:+47 73594239, e-mail: **vin.tai@elkraft.ntnu.no**, **phen.chiak.see@elkraft.ntnu.no**, **marta.molinas@elkraft.ntnu.no**

[2] ENSEEIHT
31071 Toulouse Cadex 7 (France)
e-mail: **sebmerle1987@gmail.com**

Abstract. This paper presents the study of power extraction and control of the electric power take off of a buoy type point absorber wave energy converter in heave. Two fundamental linear control strategies (the passive loading and optimum control) have been studied and their impacts on the sizing of generator were investigated. For the designed incident wave, a gearbox is needed to reach the rated speed of the generator. The generator is connected to the grid through a back-to-back converter which controls the electrical torque. Vector control technique is implemented to control the electric torque of the generator, by setting the direct axis current to zero. The results show that the current needed to control the electrical torque is too high for optimum control strategy. A method has been presented to reduce the power ratio significantly, but also with a decrease in average extracted power.

Key words

Wave energy converter, control strategy, point absorber, power take off, vector control

1. Introduction

Ocean wave energy possesses high potential to serve as one of the major supplies of energy to sustain the future world energy demands that is renewable and clean. About 2000TWh/year (or 10% of the world energy consumption) can be obtained by exploiting the wave energy potential [1]. According to the European Ocean Energy Roadmap 2010-2050 [2], wave power is expected to fulfil the EU-27 electricity demand by 0.3% in 2020 and 15% in 2050, respectively.

Currently, the ocean wave energy is at its early stage of development although the research activity in this area has been intensified in recent years. Extensive attentions have been paid to the investigation of suitable control strategies for WECs to optimise its power extraction capability. This is known as one of the key factors to the success of a WEC concept. The current primary focus of such activities is on the search for the reliable energy extraction system to fulfil the technology as well as the economical viability [3]. Several remarkable technologies have been investigated, and some of them are near to technological readiness.

To date, the design and development of such system has involved extensive studies on the mechanical and the hydrodynamic aspects while little attention has been given to the power take-off (PTO) systems [3],[4]. This causes the PTO and electrical components installed on WEC are generally oversized, in order to achieve the desired power extraction capacity. This clearly indicates a gap to be filled, to keep up with the pace of the development of the hydrodynamic models. The adoption and the proper choice of control strategies and dimensioning of the power electronic components can help in achieving an effective performance (in which the maximum power could be extracted from the ocean wave), hence further reduce the overuse of the PTO and the cost incurred in the hardware. This way, the economical viability of these systems for use in the real field operation can be increased.

This paper describes the recent work conducted by the authors in studying the impact of WEC control strategies on the generator sizing and vector control for its torque control. After briefly introducing the modelling of the WEC, an overview of the control strategies is presented along with the electrical-mechanical equivalent model. Then, the sizing of the generator is done for each of the respective control strategies. Following that, the vector control of the generator is analysed to help rating the power electronic components. The trade-off between the extracted power and the control strategies is then presented.

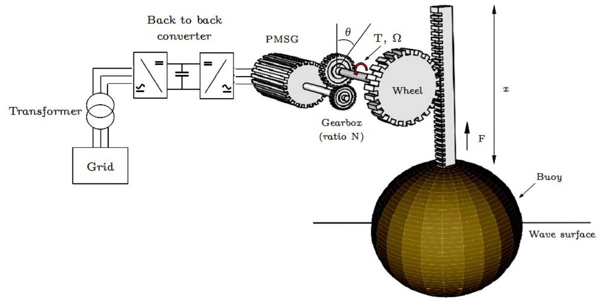

Fig. 1. Illustration of the mechanism of the WEC system

2. Modelling of the Point Absorber WEC

A. Hydrodynamic Model for WEC

The WEC model used in this study is shown in Fig. 1. Its primary extraction mechanism is a buoy which acts as a point absorber. The buoy is assumed to move linearly in heave, and its linear motion is transformed into rotational motion through a wheel (radius = 0.2m) and is amplified by the gear assembly in the gearbox. The rotational motion of the wheel is then transferred to the electrical generator through a shaft. The Permanent Magnet Synchronous Machine (PMSM) is used because of its good power coefficient and efficiency. The generator is then connected to the grid using a back to back converter. The buoy is operating under the assumption of sinusoidal waves, and the motion of the buoy is comparatively small. The plane progressive waves propagating in an infinite water depth are considered, and the horizontal coordinate of the plane is always fixed to zero. The hydrodynamic forces acting as a response to the wave based under the above assumptions can be derived [5] as follows:

$$(M+a(\omega))\ddot{x}+(B+b(\omega))\dot{x}+Kx=F_E-F_e \qquad (1)$$

$$F_e=B_e\dot{x}+M_e\ddot{x} \qquad (2)$$

Where F_E is the excitation force and F_e is the force applied by the PTO which can be externally controlled. The ω in (1) is the angular frequency of the wave. M is the mass of the WEC and $a(\omega)$ is the added water mass involved in the WEC movement at the considered frequency. B and K are the mechanical damping and hydrodynamic stiffness of the WEC, respectively. B_e and M_e in (2) are the damping and added mass applied by the PTO, respectively. x in both equations represents the position of the buoy and overdot denotes the time derivative operation. As the wave is assumed to be oscillating in sinusoidal manner, the value of x can be expressed as in (3), where $\hat{X}$ is the maximum position of the buoy, and φ_x is the initial phase angle.

$$x=\hat{X}\sin(\omega t+\varphi_x) \qquad (3)$$

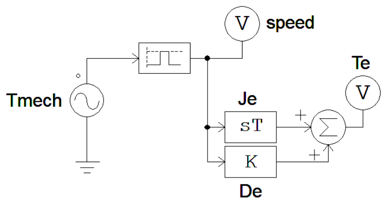

Fig. 3. Transfer function model of equation (7).

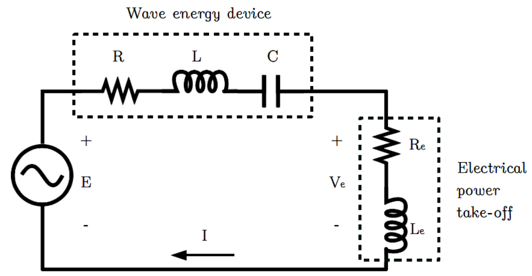

Fig. 2. Electrical analogue of a buoy type WEC

B. Mechanical Model and Electrical Analogue of WEC

As the PTO electrical machine is rotational, it is useful to rewrite the above equations in the angular forms. By introducing the definition of angular velocity and torque, (1) and (2) yield the followings:

$$(J+j(\omega))\dot{\Omega}+(D+d(\omega))\Omega+X\int\Omega=T_E-T_e \qquad (4)$$

$$T_e=D_e\Omega+J_e\dot{\Omega} \qquad (5)$$

Where T_E and T_e are the torques from F_E and F_e, respectively. Ω is the angular velocity of the PTO shaft. The rest of the parameters in (4) and (5) are defined as:

$J=r^2M$, is the global inertia of the WEC
$j(\omega)=r^2a(\omega)$, is the inertia of the added mass
$D=r^2B$, is the global damping of the WEC
$d(\omega)=r^2b(\omega)$, is the radiation resistance
$X=r^2K$, is the torsional stiffness of the WEC
$D_e=r^2B_e$, is the damping created by the PTO
$J_e=r^2M_e$, is the inertia created by the PTO

The electrical analogue of the mass-spring-damper system described by (4) is modelled as in Fig. 2. The circuit comprises two essential parts; the component that represents the buoy, and the component that represents the PTO. The equivalent components are listed in Table I.

C. Model Simplification

Also, equations (4) and (5) derived in the previous section can be rewritten in the S domain by using the Laplace transform, and following equation can be obtained:

$$J_{eq}s\Omega(s)+D_{eq}\Omega(s)+X\frac{\Omega(s)}{s}=T_E(s) \qquad (6)$$

Where J_{eq} is the equivalent inertia, which is the sum of J, $j(\omega)$, and J_e; and D_{eq} is the equivalent damping, which is the sum of D, $d(\omega)$, and D_e. The model has become simple with only one input (the angular speed) and one output (excitation torque). It has therefore, become a second order transfer function, as shown in (7). The model that represents the transfer function is presented in Fig. 3.

$$\frac{\Omega(s)}{T_E(s)}=\frac{k\,B\,s}{s^2+B\,s+\omega_0^2} \qquad (7)$$

With, $\omega_0=\sqrt{X/J_{eq}}$, $B=D_{eq}/J_{eq}$, and $k=1/D_{eq}$.

Table I. - Mechanical-Electrical Equivalence for the WEC

Mechanical Domain		Electrical Domain	
Quantity	Symbol	Quantity	Symbol
PTO angular speed	Ω	Current	I
Excitation torque	T_E	Voltage source	E
WEC global inertia	$J+j(\omega)$	Inductance	L
WEC global damping	$D+d(\omega)$	Resistance	R
WEC stiffness	X	Inverse Capacitance	$1/C$
PTO torque	T_e	Load voltage	V_e
PTO inertia	J_e	Load inductance	L_e
PTO damping	D_e	Load resistance	R_e

3. Control Strategies and Generator Sizing

Three primary control strategies have been widely investigated for WEC control [3]. They are: i.) optimum (or reactive) control, ii.) passive loading, and iii.) latching control. Optimum control and passive loading are chosen as the main subjects for this paper, due to the assumption made that the interaction between the point absorber and the wave is linear. Latching control is not covered as it is essentially an intrinsically non-linear control strategy that is beyond the scope of this study (readers who are interested in the latching control strategy are directed to [6] for more information).

The optimum control basically controls both the amplitude and the phase of the buoy's motion to achieve resonance. This generally requires the PTO system to apply a force having a component which proportional to the buoy's acceleration in addition to the component proportional to the buoy's velocity. On the other hand, the passive loading controls only the amplitude of the motion to maximize the power extraction capability. This is achieved by modifying the WEC dynamical resistance (or damping factor) using a force created by the PTO, which is proportional to the buoy's velocity. The peak to average power ratio (henceforth the power ratio) can be expressed as a function of load power factor [3], as shown in (8). It shows that the lowest possible value attainable is 2 for passive loading which always guarantees $\varphi_e=0$. On the other hand for optimum control the ratio can be very high, depending on the values of L_e and R_e used in the control.

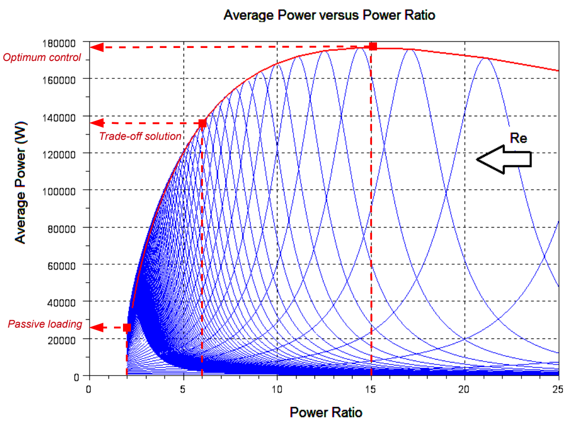

Fig. 4. Average extracted power as a function of power ratio, for several values of load resistance, R_e.

Table II. - Wave and Buoy Data

Quantity	Symbol	Unit	Value
Design wave amplitude	A	[m]	0.5
Design wave period	T	[s]	9
Buoy radius	r	[m]	5
Buoy mass	M	[kg]	268340
Added mass at considered frequency	a	[kg]	202700
Spring stiffness	K	[N/m]	789740
Total buoy damping	B	[Ns/m]	57400

The general equation for average extracted power as a function of R_e and power factor is given in (9).

$$\frac{\hat{P}}{\bar{P}}=\frac{1+\cos\varphi_e}{\cos\varphi_e} \tag{8}$$

$$\bar{P}=\frac{E^2 R_e}{(R+R_e)^2+\left(\omega L-\frac{1}{\omega C}\pm\frac{R_e\sqrt{1-\cos^2\varphi_e}}{\cos\varphi_e}\right)^2} \tag{9}$$

$$L_e=\pm\frac{R_e}{\omega}\frac{\sqrt{1-\cos^2\varphi_e}}{\cos\varphi_e} \tag{10}$$

Fig. 4 presents the average extracted power as a function of power ratio, obtained by using (8) and (9) across a number values of load resistances. The parameters of the buoy chosen for this study are in accordance with the device described by [7], as in Table II. With the aid of Fig. 4, the maximum average extracted power available in resonance condition can be found, alongside with its corresponding value of R_e. Its corresponding value of L_e is calculated from (10). Note that the +/- sign in (9) and (10) depends on the inductive or capacitive nature of the equivalent load. The results are reported in Table III.

The parameters obtained in Table III are fed into the simulation model in PSIM as shown in Fig. 3. The corresponding curves of the electrical PTO torque, T_e and the mechanical speed, Ω are presented in Fig. 5 and Fig. 6, for passive loading and optimum control, respectively. The mechanical power, which is the product of Ω and T_e are also presented.

The torque generated by PTO is proportional to the PTO speed, and the resultant power from the PTO is always positive for passive loading, indicating that the PMSM is working only in generation mode. The transient is quick, as steady state is reached after the first oscillation. The maximum values of the power and speed are 47.29 kW and 1.21 rad/s (11.55 rpm), respectively, in steady state. The maximum speed is very low for a PMSM. Therefore, a gearbox with a ratio of 50 is needed to fit in a 600 rpm

Table III. - Equivalent circuit components and power ratio of respective control strategies

Parameters [Unit]	Passive Loading	Optimum Control
$\hat{P}/\bar{P}$	2	15
R_e [Ω]	804420	57400
L_e [H]	0	1149300

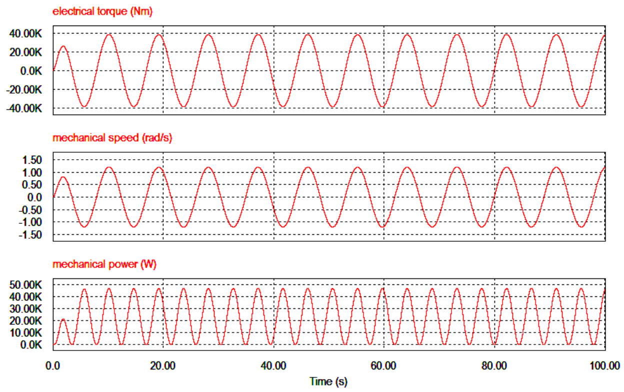

Fig. 5. Mechanical speed, electrical torque, and mechanical power attainable with passive loading.

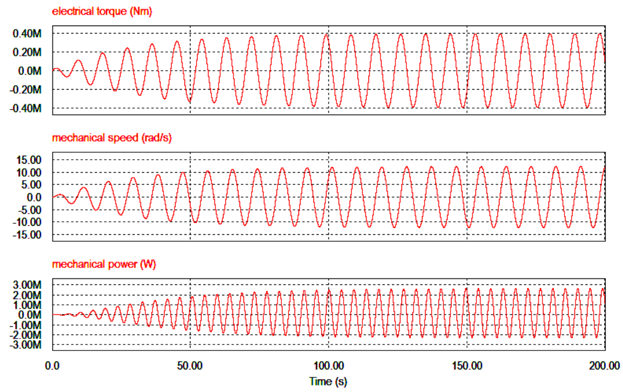

Fig. 6. Mechanical speed, electrical torque, and mechanical power attainable with optimum control.

rated speed PMSM. For simplicity, the gear system is assumed to be frictionless. The average extracted power for this control strategy is 23.65 kW.

For optimum control, the torque generated by PTO is not proportional to the PTO speed. The power changes sign regularly and the PMSM alternates between generator and motor modes. The transient state is long as steady state is reached after 100 seconds. High amplitudes of power, torque, and speed are observed (2.66 MW, 400 kNm, and 12.5 rad/s, respectively) in steady state, due to the fact that the WEC is operating in resonant condition. A four-pole PMSM with rated speed of 1500 rpm is chosen for this control strategy. A gear ratio of 12 is needed to reach 1500 rpm at the PTO output from 119.4 rpm (12.5 rad/s). The average extracted power is 176.93 kW.

The analysis done so far without taking into account the effect of PMSM. Knowing the moment of inertia, J_G and the damping factor, D_G of the PMSM, the equivalent moment of inertia and equivalent damping factor in (6) are modified, to include the inertia, $N^2 J_G$ and damping, $N^2 D_G$ brought by the PMSM. The electrical parameters of the PMSM of both control strategies are presented in Table IV. Non-salient pole PMSM is assumed in this paper. The inertia and damping of the generator are 0.1 kgm^2 and 0.001 Nms, respectively. The average extracted power found without neglecting the inertia and damping of the PMSM for passive loading and optimum control are 23.65 kW and 176.65 kW, respectively. Compare with the results obtained earlier, the differences are less than 1%. The effect inertia and damping of PMSM on WEC is thus negligible. The corresponding values of L_e and R_e for optimum power extraction are also very close to the ones obtained without considering the effect of PMSM. The results are presented in Table V.

Table IV. - Electrical parameters of PMSM for passive loading and optimum control.

Parameter [unit]	Passive loading	Optimum control
R_s [Ω]	0.1413	0.00255
L_d [H]	0.0156	0.7060
L_q [H]	0.0156	0.7060
$V_{pk}/krpm$ [V]	1626.3	650.5
Number of poles, p	10	4
Gear ratio, N	50	12

4. Vector Control for PMSM

The power extracted in the previous section is channelled to the grid through a back-to-back converter, which consists of a rectifier and an inverter connected to a common DC-link. The rectifier connected to the PMSM is controlled according to the aforementioned control strategies. The inverter converts the DC voltage from the DC-link into AC voltage before the power is being transferred to the grid. As this paper is focused on wave power extraction, only the rectifier side of the converter is considered. Since the DC-link voltage is to be held constant at all time, it can be approximated as a constant voltage source as shown in Fig. 7. Speed sensor is used to measure the mechanical speed, ω_{mech} of the generator shaft. The mechanical angle of the shaft, θ_{mech} is then obtained through integration. These values are then multiplied by the number of pole pairs to obtain the electrical speed, ω_e and electrical angle, θ_e, respectively. Current sensors are integrated at the PMSM output to control the current. The d-axis current, $\boldsymbol{i_d}$ and q-axis current, $\boldsymbol{i_q}$ are obtained through the transformation matrix as described in (11).

$$\begin{bmatrix} i_d \\ i_q \\ i_o \end{bmatrix} = \frac{2}{3} \begin{bmatrix} \cos(\theta_e) & \cos(\theta_e - 2\pi/3) & \cos(\theta_e + 2\pi/3) \\ \sin(\theta_e) & \sin(\theta_e - 2\pi/3) & \sin(\theta_e + 2\pi/3) \\ 1/2 & 1/2 & 1/2 \end{bmatrix} \begin{bmatrix} I_1 \\ I_2 \\ I_3 \end{bmatrix} \quad (11)$$

The control of the electrical PTO torque can be done by setting the d-axis current to zero. In the PMSM d-q synchronous reference frame, the electrical PTO torque can be expressed as in (12). ψ_{PM} is the flux linkage of the permanent magnet.

$$T_e = N \frac{3}{2} \frac{p}{2} \psi_{PM} i_q \quad (12)$$

Table V. - Adjusted control parameters and PMSM performances for optimum power extraction.

Parameter [unit]	Passive loading	Optimum control
R_e [Ω]	800100	57436
L_e [H]	0	1149000
$\bar{P}_e$ [kW]	23.65	176.65
$\hat{P}_e$ [kW]	47.3	2649.9
Power ratio	2	15

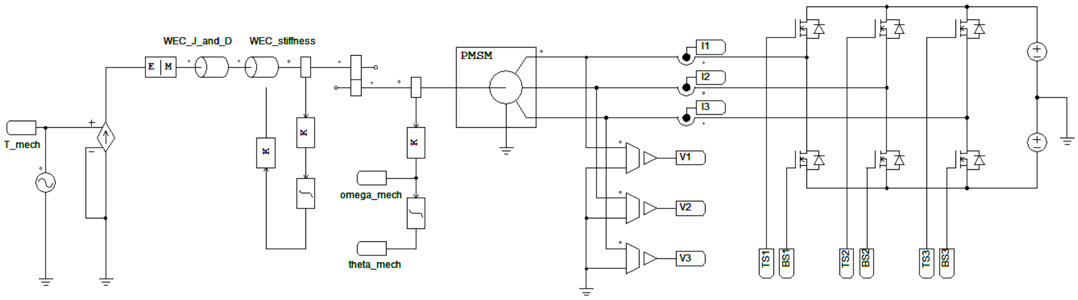

Fig. 7. Schematic of the investigated system.

Also in d-q reference frame, the output voltages of the PMSM are given by (13) and (14). However the equations are cross coupled. A simple solution to tackle this cross coupled situation is to consider a different voltage reference with the cross coupling terms, as shown in (15) and (16). U_d and U_q are the d and q axes voltage references, respectively. This makes the transfer function between U_d and i_d, as well as the transfer function between U_q and i_q become linear.

$$V_d = R_s i_d + L_s \frac{d\, i_d}{dt} - \omega_e L_s i_q \tag{13}$$

$$V_q = R_s i_q + L_s \frac{d\, i_q}{dt} + \omega_e L_s i_d + \omega_e \psi_{PM} \tag{14}$$

$$U_d = V_d + \omega_e L_s i_q \tag{15}$$

$$U_q = V_q - \omega_e L_s i_d - \omega_e \psi_{PM} \tag{16}$$

The identification of the parameters of the PI controller for the currents can now be estimated. The time constant of the PI controller compensates the electrical time constant. The gain, K_p of the PI controller is chosen to keep the phase margin, M_φ to 66° for stability. The transfer function in open loop, $TF_{OL}(s)$ of i over U for both d and q components including the delay, T_a brought by the converter and the PI controller after the pole compensation is as follows:

$$TF_{OL}(s) = \frac{i(s)}{U(s)} = \frac{K_p}{(1 + T_a s/2) L_s s} \tag{17}$$

with,

$$\omega_{0db} = 2 \tan(180^o - M_\varphi - 90^o)/T_a$$

$$K_p = \omega_{0db} L_s \sqrt{1 + (\omega_{0db} T_a/2)^2}$$

The control circuit is set as shown in Fig. 8. The voltage components V_d and V_q are found from (15) and (16) by compensating the cross coupling terms. Reverse d-q

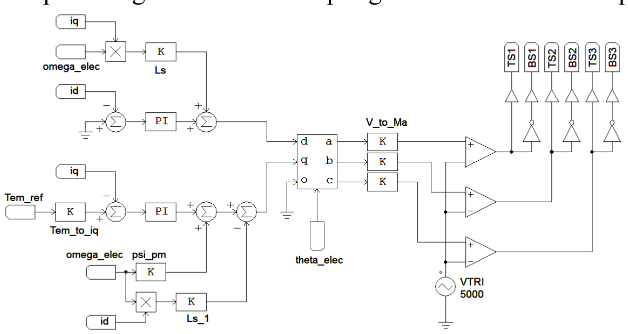

Fig. 8. Schematic of the vector control circuit with the PWM.

transformation is applied to obtain the line voltage references V_1, V_2, and V_3, to control the PWM of the rectifier connected to the DC-link. The simulation results of speed and currents, along with their reference values are plotted in Fig. 9. and Fig. 10. for passive loading and optimum control, respectively. The output power of the generator, P_e is obtained by using (18).

$$P_e = V_1 I_1 + V_2 I_2 + V_3 I_3 \tag{18}$$

For passive loading, the speed aligns perfectly with the reference speed. The d-axis and q-axis currents are also well aligned with the reference currents, but they present a ripple of around 2 A. This ripple is negligible compare with the amplitude of the oscillation. The extracted power is always positive. This confirms that the PMSM is operating only in generator mode. The average power obtained gives the same results as the one computed analytically in the previous sections. The control is thus validated.

For optimum control strategy, the speed and the d-q axes currents are also aligned well with their references. The q-axis current presents a resonance oscillation and surpasses

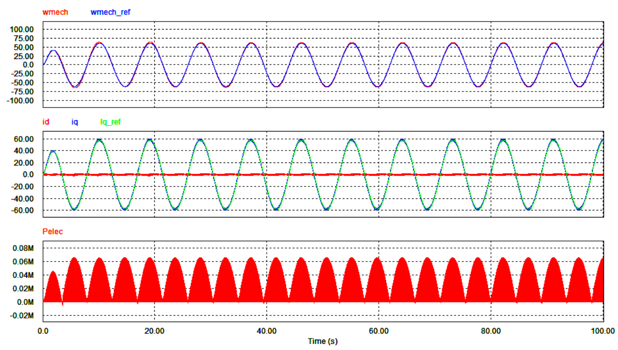

Fig. 9. Simulation results of speed, currents, and instantaneous power for passive loading strategy.

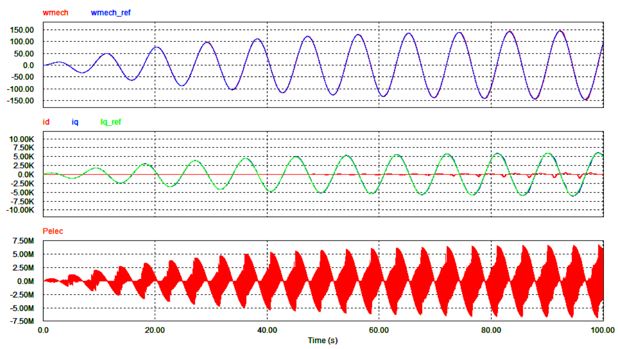

Fig. 10. Simulation results of speed, currents, and instantaneous power for optimum control strategy.

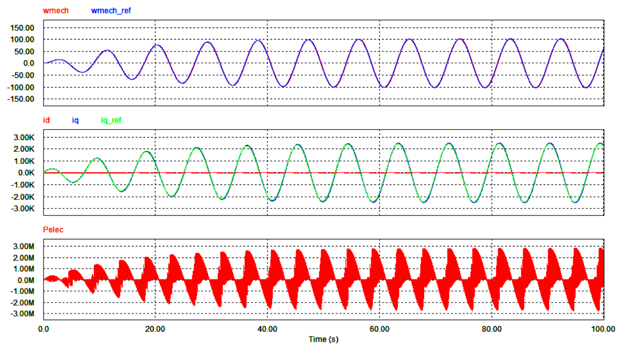

Fig. 11. Simulation results of speed, currents, and instantaneous power for trade-off control solution.

5 kA in less than 50s. This value is too high for torque control as compared with the rated current of the generator, which is only 3.3 kA by assuming the rated voltage of the generator is 690 V which can be commonly found in the market. A solution to this is to consider an overrated generator to increase the current capacity but it is not an optimised solution. Another alternative is by designing a torque control saturation to saturate the current. The extracted power changes sign alternately. This confirms that the machine is working in generator and motor modes, alternately.

5. Trade-off Control Strategy Solution

The generator and power electronics have to to be rated very high with optimum control, which makes it difficult to implement. Therefore the power ratio has to be reduced for a more suitable dimensioning of the electrical components. Meanwhile, the dimensioning for passive loading is not a problem as the peak power and average power is comparatively low. With the use of Fig. 4., a more proper value of power ratio can be determined. The power ratio is chosen to be 6 in this study. Its corresponding average power is 136.5 kW, which is about 77% of the power available with the optimum control strategy. It is a small reduction compared to the improvement of the power ratio, which is reduced by 60%. Choosing an even smaller power ratio to use a particular generator will also yield a smaller average power extraction. The simulation results for the trade-off solution are presented in Fig. 11. The measured speed and current match perfectly with the reference speed. The machine is working in generator and motor modes alternately. Compared with the optimum control case, the amplitude of the q-axis current has been reduced to less than the rated current of the generator. As described by (14), this strategy is also a good solution to reduce the electrical torque.

6. Conclusions

The linear model used in this study is valid when monochromatic waves are assumed. The control presented here for the specific PTO needs yet to be tested under the real sea conditions, as for example in [8]. The amount of power available to be extracted for each control strategy is obtained by using the analytical equations presented by [3]. For the designed wave, it has been shown that a gearbox is needed for each control strategies to reach the rated speed of the PMSM. This is also true for irregular waves comprised by a large number of sinusoidal waves with various frequencies, where a gearbox with variable gear ratios could be devised as a solution.

A mechanical model with PMSM has been set up in PSIM to verify the results obtained analytically. The rating of the generator depends on the peak power value from the previous analysis. Then the power electronic converter and its vector control were implemented in the model. The current control loop controls the electrical torque of the generator according to the selected control strategy. The vector control for passive loading worked perfectly but the power extracted is rather low. The advantage of passive loading is the reasonable rating of the generator and power electronic converter components. For optimal control however, the current required to control the electrical torque is higher than the rated current of the generator, due to high power ratio of WEC operating in resonant condition.

A trade-off solution has been proposed to obtain the parameters for the torque control that would give a lower power ratio with acceptable reduction in average extracted power. The results obtained from the proposed method showed a significant reduction in the current needed for electrical torque control and also the rating of the generator. The currents also presented a ripple of about 2 A, which is small and can be smoothed by using a filter at the output of the machine.

The authors suggest the continuation of this work in the area where the irregularity of the ocean wave as well as the valid real-time wave pattern prediction is taken into account.

References

[1] T. W. Thorpe, "An Overview of Wave Energy Technologies: Status, Performance and Costs", in Wave Power – Moving Towards Commercial Viability, IMECHE Seminar, London, 30 November 1999.
[2] European Ocean Energy Association, "Ocean of energy: European ocean energy roadmap 2010-2050", Imprimerie Bietlot, Belgium, 2010.
[3] E. Tedeschi, and M. Molinas, "Impact of control strategies on the rating of electric power take off for wave energy conversion", IEEE Int. Symp. Ind. Electron., Bari, 2010, pp. 2406-2411.
[4] J. Cruz, "Ocean wave energy: current status and future perspectives", Springer, Berlin, 2008.
[5] J. Falnes, "Ocean waves and oscillating systems: linear interactions including wave-energy extraction", Cambridge Univ. Press, Cambridge, 2002.
[6] J. Hals, "Modelling and phase control of wave-energy converters", PhD dissertation, Dept. Marine Tech., Norwegian Univ. Tech. and Sci., Trondheim, 2010.
[7] J. Hals, T. Bjarte-Larsson, J. Falnes, "Optimum reactive control and control by latching of a wave-absorbing semisubmerged heaving sphere", Proc. 21st Int. Conf. Offshore Mech. and Artic Eng., Oslo, 2002, pp.1-9
[8] E. Tedeschi, M. Molinas, M. Carraro, and P. Mattavelli, "Analysis of power extraction from irregular waves by all-electric power take off", IEEE Energy Conversion Congr. and Expo., Atlanta, 2010, pp. 2370-2377.